INTERNATIONAL JOURNAL OF CLIMATOLOGY
Int. J. Climatol. **20**: 939–953 (2000)

THE RELATIONSHIP BETWEEN THE SIMULATED CLIMATIC VARIABILITY MODES OF THE TROPICAL ATLANTIC

JACQUES SERVAIN[a,*], ILANA WAINER[b], HERVÉ LUDOS AYINA[a] and HERVÉ ROQUET[c]
[a] *Centre IRD de Bretagne, BP 70, 29280 Plouzané, France*
[b] *Dept. Oceanográfia Fisicá, Universidade de São Paulo, São Paulo, Brazil*
[c] *CMS, Météo-France, Lannion, France*

Received 28 June 1999
Revised 4 October 1999
Accepted 4 October 1999

ABSTRACT

Two main modes of climatic variability occur in the tropical Atlantic Ocean at inter-annual time-scales: the equatorial mode, similar to the El Niño phenomenon in the Pacific Ocean, and the meridional mode, or dipole-like mode, with no Pacific counterpart. The Atlantic equatorial mode is characterized by the occurrence of alternating warm and cold episodes at the equator, on the eastern side of the basin. These events are associated with abnormal variations in the zonal equatorial slope of the thermocline. The meridional mode is characterized by an inter-hemispheric gradient in the sea-surface temperature (SST). The mean position of the Inter-tropical Convergence Zone (ITCZ) separates positive and negative SST signals. It was recently shown with observational indices that there is significant correlation between these two climatic modes of variability. This study goes one step further, by using a multi-year numerical simulation, where an oceanic general circulation model is forced by the 1979–1993 ECMWF reanalysis. Model computed indices representing the two main modes of variability compare well with observations. The two inter-annual modes of variability are shown to have the same physics as the annual variability does, which is related to the latitudinal displacement of the ITCZ. Furthermore, it is suggested that the ocean dynamics (as opposed to thermodynamic processes) is the principal cause of climate variability in the region. Copyright © 2000 Royal Meteorological Society.

KEY WORDS: climatic variability; temperature; thermocline depth; tropical Atlantic

1. INTRODUCTION

Inter-annual variability in the tropical Atlantic Ocean is often regarded as being dwarfed by the powerful influence of the annual cycle (Merle *et al.*, 1980). However, it has been established that large anomalous deviations from the annual cycle appear in the ocean–atmosphere system at various time-scales (from a few months to many years), primarily for the sea surface temperature (SST), even if the range of the SST anomalies remains smaller with respect to the range of the seasonal variability (Servain *et al.*, 1985). Previous studies have shown that the ocean–atmosphere inter-annual variability in the tropical Atlantic can be represented by two main modes: a shorter time-scale mode (a few months), similar to El Niño in the Pacific Ocean (e.g. Zebiak, 1993), which manifests itself primarily near the equator and inside shallow waters; and a longer time-scale mode (many years), which has no counterpart in the Pacific. The latter mode is also known as the 'Atlantic dipole' mode (e.g. Hastenrath, 1978; Servain, 1991; Servain *et al.*, 1998a). It is characterized by a north–south inter-hemispheric gradient in SST. Very recently, Servain *et al.* (1998b, 1999) have shown using observations that these two main modes appear to be linked statistically in the inter-annual frequency band. The aim of this paper is to reinforce and complete this previous result by using a new set of simulated data.

* Correspondence to: Centre IRD de Bretagne, BP 70, 29280 Plouzané, France; tel.: + 33 298224506; fax: + 33 298224514; e-mail: servain@ird.fr

The scientific approach is based primarily on diagnostic comparisons during common periods between available observed and simulated datasets. Efforts are conducted from space–time averaged patterns, and from empirical orthogonal function (EOF) analyses. Both surface and subsurface oceanic variables are analysed. Surface oceanic variability is observed through the SST fields, and the 20°C isotherm depth (noted here as Z20) is chosen to give an idea of the upper-ocean variability. The depth of the 20°C isotherm is commonly identified in the tropical regions as being representative of the centre of the main thermocline, which is the depth at which temperature variations are the greatest (Merle and Arnault, 1985; Houghton, 1991; McPhaden, 1993; Smith and Chelliah, 1994). Thus, Z20 is a good indicator of the depth of the upper-warm layer in the tropical Atlantic Ocean.

The overall organization of this paper is as follows. Section 2 is a brief summary of the characteristics of the two main modes of inter-annual oceanic variability, as well as an update of their recently appointed relationship from observations (Servain *et al.*, 1998b, 1999). Section 3 describes the simulated dataset used in this study, and discusses the ability of the oceanic numerical solution to reproduce the main modes of variability and their relationship. This section also suggests that the dynamics linked to the perturbations of the whole trade winds system are of prime importance for the generation of the two observed modes of oceanic variability, thus inducing their relationship. Section 4 concludes the paper.

The monthly anomaly times series used in this paper are related to the period 1980–1997 for the observations and the period 1979–1993 for the numerical solution. The degrees of freedom used to determine their cross-correlation were obtained by dividing the total record lengths (216 and 180 months, respectively) by the integral time period needed to obtain two independent realizations (autocorrelation coefficients close to zero after about 6 months). This induces that a correlation coefficient up to 0.42 and 0.45, for the 1980–1997 and 1979–1993 periods, respectively, are significant at the 5% level.

2. THE MODES OF INTER-ANNUAL VARIABILITY IN THE TROPICAL ATLANTIC

2.1. Equatorial mode

Equatorial waves and remote wind forcing play a significant role in the tropical Atlantic in the generation of surface and subsurface thermal anomalies on the inter-annual time-scale. In other words, wind perturbations in the western equatorial Atlantic Ocean trigger eastward Kelvin waves that travel east across the basin, for up to weeks, to be reflected westward from the African coast as slower equatorial Rossby waves. At the same time, part of the incoming Kelvin wave gets trapped at the coast, travelling polewards and triggering an east–west response at latitudes away from the equator. Therefore, this equatorial perturbation will be felt at off-equator latitudes later than the initial wind disturbance in the west equatorial region. Certain dynamical aspects of equatorial wave reflection off the eastern Atlantic Ocean are complex and will not be the focus of this study. The reader is referred to, for instance, Moore *et al.* (1978), Philander (1979) and McCreary *et al.* (1984), for a theoretical overview of equatorial dynamics, and to Picaut (1983) and Katz (1987, 1997) for observational evidence. The equatorial adjustment phenomena can be well simulated and understood with very simple linear models (e.g. Servain and Arnault, 1995). Significant examples of the appearance of the equatorial mode are the warm events of 1968, 1984, 1995, and more recently, 1997–1998. Important cold events were noted in 1967, 1976 and 1978.

Such inter-annual events have important local climatic and socio-economic consequences, as, for instance, those affecting open ocean tuna fishing efforts (Fonteneau, 1991), as well as distribution of several pelagic species along the African coast (Binet, 1982; Binet and Marchal, 1993). Adjacent coastal areas also feel the impact of varying ocean temperatures, such as changes in the regional distribution and intensity of precipitation (Carton and Huang, 1994; Wagner and da Silva, 1994). For example, during the warm event of 1968, strong rains led to flooding in several African countries that border the Gulf of Guinea (Hisard, 1980).

2.2. Meridional mode

Thanks to the increasing number of surface marine observations obtained from the global meteorological network and merchant ships, the meridional mode of variability has been easily detected in the surface tropical Atlantic Ocean. Indeed, the amount of surface data is relatively high and permits a continuous temporal–spatial analysis of monthly winds and SST (Servain *et al*., 1985) on a 2° latitude × 2° longitude grid over the tropical Atlantic. The available subsurface data, which are obtained from expandable bathythermograph (XBT) drops by merchant ships on specific routes, are less numerous and their coverage is mainly restricted to the ships' tracks. Therefore, it is extremely difficult to obtain a basin-wide picture of the inter-annual variability below the surface.

The surface meridional mode involves a low-frequency oscillation of the SST gradient across the equator (Servain, 1991; Mehta and Delworth, 1995; Tanimoto and Xie, 1999). It is associated with the slow inter-annual meridional fluctuations of the mean position of the Inter-tropical Convergence Zone (ITCZ), and can be seen across several time-scales, ranging from seasonal to decadal (Servain, 1991). While air–sea interactions may be instrumental in determining the origin of the inter-hemispheric SST anomalies, other positive feedback involving dynamical processes may also play a role. Some authors, such as Chang *et al*. (1997) and Delworth and Mehta (1998), believe that decadal variations of the dipole mode originate from ocean–atmosphere positive feedback involving primarily SST and wind-induced latent heat flux. The idea is that there is a mutual interaction between the wind-induced heat flux and SST so that the SST anomalies maintain the anomalous wind pattern, and thus the surface heat flux anomalies, while ocean processes set the slow time-scale of variability.

Although there is debate as to whether the dipole mode is a physical reality or a statistical artefact (Houghton and Tourre, 1992; Enfield *et al*., 1999), it is obvious that such a type of variability is strongly related to the rainfall regime of Northeast Brazil (Nordeste) (Moura and Shukla, 1981; Servain, 1991; Harzallah *et al*., 1996; Nobre and Shukla, 1996; Wainer and Soares, 1997; Rao *et al*., 1999), as well as that of West Africa (Lamb, 1978a,b; Fontaine and Bigot, 1993; Fontaine *et al*., 1995; Moron *et al*., 1995; Wagner, 1996). Periods of increased rainfall (droughts) in Nordeste are associated with the anomalous displacement of the ITCZ towards the south (north), which frequently will correspond to an inter-hemispheric pattern of anomalous cold (warm) SST to the north and warm (cold) SST to the south. Droughts in sub-Saharan Africa (Sahel) are also often found to be associated with a broad band of negative/positive SST anomalies across the tropical north/south Atlantic, though it seems that the relationship is strongest beyond the decadal scale and almost vanishes at an inter-annual scale during the contemporaneous dry period. The link between equatorial SST anomalies and Guinean rainfall seems stronger and more stable than that with Sahelian rainfall (Moron, Personal Communication, 1999).

2.3. Observed relationship between the two modes

2.3.1. Observed dataset. The observed SST dataset was processed at Centre IRD de Bretagne (Servain and Lukas, 1990) from the Volunteer Observing Ship (VOS) raw measurements. It covers the tropical Atlantic basin from 30°N to 20°S, and from 60°W to the African coast, during 1964–1997.

The observed Z20 dataset used here was obtained from XBT observations archived at the TOGA-WOCE Subsurface Data Centre (Fabri *et al*., 1996). It covers the Atlantic region from 20°N to 20°S for the period 1985–1997. Owing to the relative paucity of the XBT data in the tropical Atlantic region (from 0 to a very rarely maximum of 9 XBT lines per month), only the ship tracks Europe–South America and Europe–South Africa (respectively designed by AX 11 and AX 15 in the TOGA-WOCE ship track list) were (nearly) continuous during the years 1980–1997, and are the only ones used in this paper. The AX 11 ship track goes through the tropical basin by a straight line from 20°N–21°W to 20°S–39°W, crossing the equator close to 30°W (Figure 1), and following the Brazilian coast southward of 5°S. The AX 15 line follows the African coast closely from 20°N to about 6°N, and steers directly to South Africa in the open ocean, crossing the equator close to 10°W. Merle (1980) has shown that the equatorial crossing points (30°W–Equator and 10°W–Equator) are dynamically connected because of their opposing western and

eastern locations. The 10°W–Equator position is particularly interesting because it is where equatorial surface variability is at its highest value (Servain *et al.*, 1985; Philander and Pacanowsky, 1981).

Within some upwelling areas and during some periods of the year, the 20°C isotherm may be missing, due to the surfacing of Z20. Thus, on AX 15, Z20 is missing for about 20% of the XBT data north of 13°N, and for 20–80% during the austral winter south of 13°S.

Two types of monthly anomalies are used in this study: simultaneously for the observed and the simulated data sets. For each SST and Z20 variable, the monthly anomalies are the deviations of the monthly means from the monthly climatology. They are used here to compare the model results from the observations quantitatively and qualitatively at the same locations. These quantities are expressed in °C and in metres, respectively. The standardized monthly anomalies are the former anomalies divided by their monthly standard deviations. They are used here to compare monthly anomaly time series spatially averaged over two different domains. Both types of analyses allow the seasonal signal, which is obviously out of phase between the two hemispheres, to be removed. They also allow the withdrawal of any spurious bias of the model results versus the observations, both in the mean state or in the mean seasonal cycle.

2.3.2. The observed relationship between the two modes. The equatorial mode is characterized by changes in the slope of the equatorial thermocline, while the dipole mode is characterized by inter-hemispheric SST

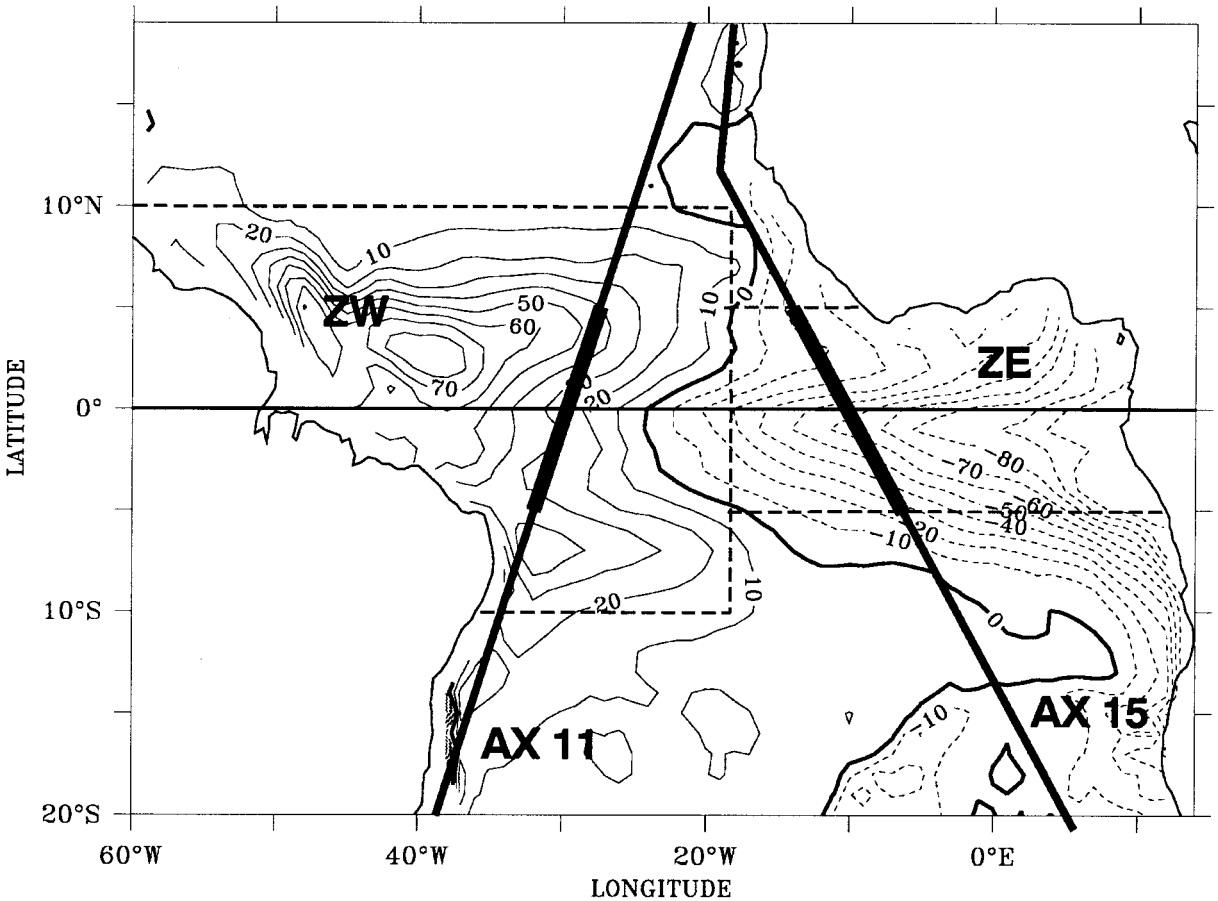

Figure 1. Spatial structure of EOF-1 of the simulated Z20 monthly anomaly. Thick straight lines indicate ship tracks AX 11 (west) and AX 15 (east), super thickened from 5°N to 5°S (see also Figure 3). Thick dashed lines indicate the limits of ZW and ZE areas used in Figure 8 to calculate an ΔZ20 simulated index. Contour interval (positive in solid lines, negative in dashed lines) is 10 in standard units

anomalies with opposite signs on either side of the ITCZ. As in Servain *et al.* (1998b, 1999), the 1980–1997 XBT data are used with the annual cycle removed along the AX 11 and AX 15 ship tracks, to estimate the equatorial thermocline slope from observations. These time series are averaged from 5°N to 5°S along the two ship tracks (see Figure 1), giving Z20 close to 30°W for AX 11, and close to 10°W for AX 15. The difference between these two records is a measure of the equatorial thermocline slope, ΔZ20. Positive (negative) values of ΔZ20 correspond to a rather pronounced (rather flat) thermocline slope.

To measure the inter-hemispheric SST gradient, ΔSST, the differences between anomalous SSTs averaged from 20 to 5°N (TN) and from 5°N to 15°S (TS) were used. These two domains are shown in Figure 2. That procedure, which is consistent with the computation of ΔZ20, is similar to that in Servain (1991) for his Atlantic dipole index, with the difference that the poleward limits are 28–20°N and 20–15°S, respectively. Positive (negative) values of ΔSST correspond to a SST dipole pattern that is warm (cold) in the northern ocean and cold (warm) in the equatorial and southern regions.

The two observed indices, ΔZ20 and ΔSST, are plotted in Figure 3. The maximum correlation coefficient (MCC) between them is 0.45 with a 2-month lag (ΔZ20 leading). This implies that the equatorial and dipole modes are linked at inter-annual time scales. In their analyses of inter-decadal and inter-annual oscillations in global SST, Moron *et al.* (1998) also suggest that the modulation of inter-annual variability around the Atlantic can be linked to other longer time-scales phenomena, such as the inter-hemispheric SST gradient. In fact, the coherence between ΔSST and ΔZ20 is at its highest

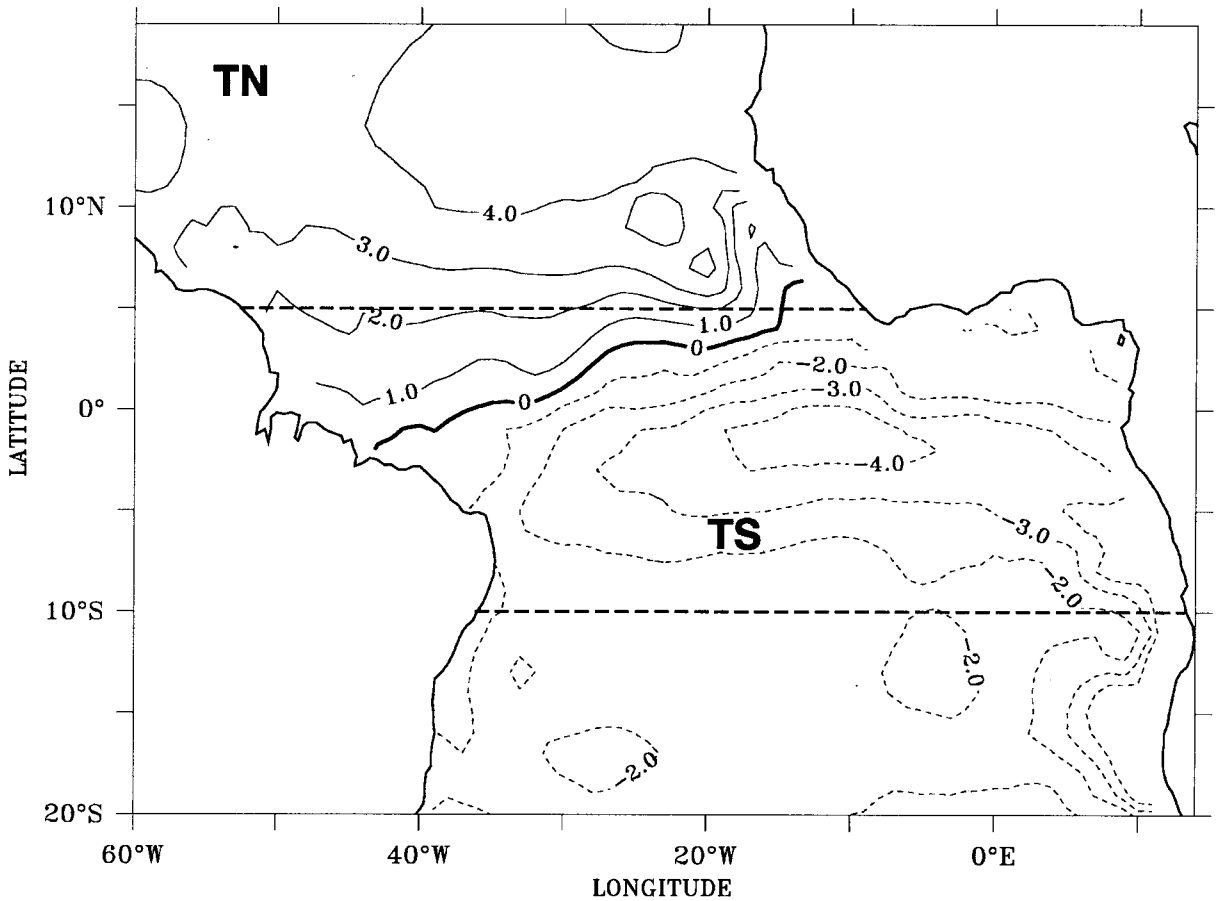

Figure 2. Spatial structure of EOF-1 of the simulated SST monthly anomaly. Thick dashed lines indicate the limits of the TN and TS areas used in Figure 3 and Figure 8 to calculate observed and simulated ΔSST indices, respectively. Contour interval (positive in solid lines, negative in dashed lines) is 1 in standard units

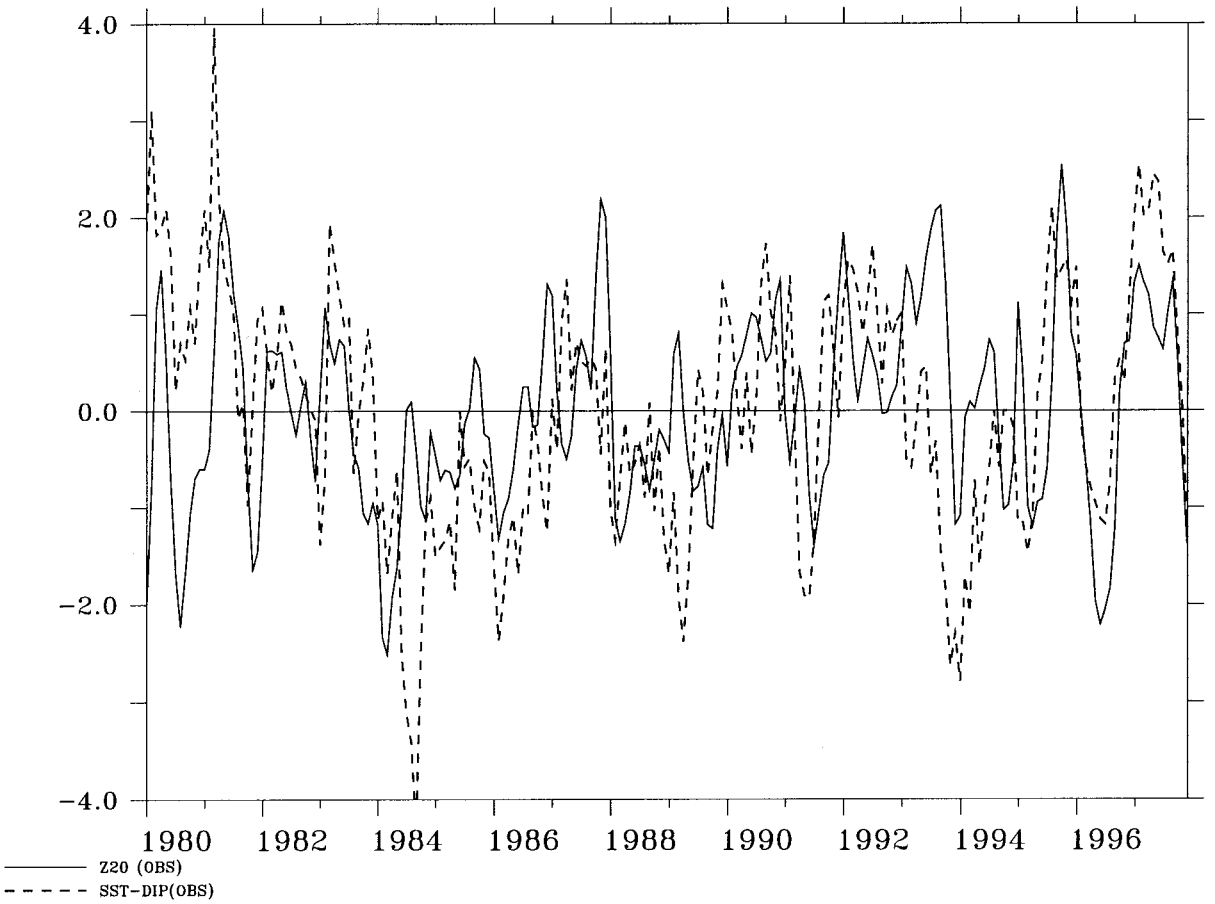

Figure 3. 1980–1997 observed monthly time series of ΔZ20 (solid line) and ΔSST (dashed line) from the observations. Here, ΔZ20 relates the difference between Z20 standardized anomalies averaged along AX 11 from 5°N to 5°S minus Z20 standardized anomalies averaged along AX 15 from 5°N to 5°S. ΔSST relates the difference between SST standardized anomalies averaged inside 20°N–5°N (TN on Figure 2) minus SST standardized anomalies averaged inside 5°N–15°S (TS on Figure 2). For both domains, the western limit is 60°W or the American coast, while the eastern limit is the African coast

on decadal and 1–3 year time-scales (Servain *et al.*, 1999). Several 2–3 year oscillations, in which the SST dipole evolves from a positive state (northern warmer than southern) to a negative state and returns, can be seen during the study period. At the same time, the tilt of Z20 along the equator oscillates between a pronounced slope ($\Delta Z20 > 0$) to a flat thermocline ($\Delta Z20 < 0$). At a very low frequency, the most pronounced feature is a slow tendency from negative values by 1984 to positive values by 1993.

3. RESULTS FROM THE SIMULATION

3.1. The simulated dataset

The oceanic general circulation model (OGCM) used in this study is the OPA7. It was developed in the Laboratoire d'Océanographie Dynamique et de Climatologie (LODYC) at the University of Paris 6, and is described elsewhere (e.g. Reverdin *et al.*, 1991; Delécluse *et al.*, 1993).

In the version used here, the OGCM covers the Atlantic Ocean from 55°N to 34°S, with a progressive relaxation to the Levitus (1982) temperature and salinity climatology north of 20°N and south of 20°S at all depths. The analysis of the model outputs is limited to the inter-tropical region (20°N–20°S), where the

model is entirely prognostic and has a maximum latitude/longitude resolution of $0.33° \times 0.5°$ at the equator, and a vertical resolution of 10 m near the surface.

The initial conditions of the OGCM were obtained from a 10-year annual cycle run, using the mean state of the model in December of the last year. Then, the OGCM was forced during the 1979–1993 period by the outputs (wind stress, sensible and latent heat fluxes, short and long wave radiative fluxes) from the ERA-15 reanalysis performed at ECMWF (Kallberg, 1995). Little sensitivity was found when choosing another month (June) from the 10-year annual cycle run as initial conditions, due to the fact that the OGCM is highly constrained by the surface forcing and the boundary conditions north of 20°N and south of 20°S. The ERA-15 fluxes were available every 6 h on a $1° \times 1°$ mesh, as produced by the ECMWF atmospheric global circulation model (AGCM) during the first 6 h of integration after each analysis time (00, 06, 12 and 18 UTC). The NCEP weekly SST analysis (Reynolds and Smith, 1994) was used by the ERA-15 reanalysis (from November 1981 onwards) as a boundary condition for the AGCM over oceans, and was also used in an additional relaxation term to constrain the temperature at the first level of the OGCM (5 m), with a constant relaxation coefficient of 40 $W m^{-2} K^{-1}$. Because of the uncertainties in the quality of the rainfall produced by AGCMs in tropical areas, no surface fresh water flux was used, and the salinity at the first level of the OGCM (5 m) was constrained only by the annual Levitus (1982) salinity climatology. The instantaneous OGCM outputs were stored for each 5-day period at each point of the oceanic model grid. According to the time-scale grid structure of the observed SST and Z20 data fields, simulated SST and Z20 were prepared on the same manner: monthly averages, $1° \times 1°$ mesh, but over a northerly restricted domain (20°N–20°S; 60°W-African continent). For the comparison between observation and simulation of Z20 along AX 11 and AX 15, only the $1° \times 1°$ squares closest to AX 11 and AX 15 and belonging to the model were selected.

3.2. The ability for the model to reproduce the seasonal to inter-annual time-scales variability

3.2.1. Comparison between simulated and observed SST and Z20. Figure 4 shows the climatic averages and seasonal ranges of SST (observed SST on Figure 4(a); simulated SST on Figure 4(b)) and Z20 (simulated Z20 on Figure 4(c)). The model is able to reproduce reasonably well the climatic averages and the seasonal amplitudes of these variables. The plots show that the location of the SST maximum and minimum of seasonal range, coincides with the thermal equator and hence the mean ITCZ position. High values of the SST seasonal range (greater than 6°C) are found in coastal and equatorial regions, where seasonal upwelling is known to occur.

Figure 4(c) is similar to Figure 4(b) but using the simulated Z20. As expected, low values of Z20 (less than 80 m) occur in the eastern basin, with high values (up to 80 m) occurring in the western region. The pattern of the climatic mean, with strong zonal characteristics, is consistent with previously known dynamics (Merle and Arnault, 1985). The seasonal variability is the highest (up to 30 m) along the equator and in the northwestern equatorial region associated with important mesoscale phenomena linked to variations in the Ekman pumping (Carton *et al.*, 1996) and fast displacements of the ITCZ. Note that at the southeastern area (south of 15°S), the Z20 surfaces seasonally making the analysis in that region difficult.

3.2.2. Correlation between SST and Z20 anomalies. Figure 5 shows that the correlation at zero lag between the simulated SST and Z20 anomalies is predominantly positive in the eastern basin, and negative in the western basin. In the east, warm (cold) SST is associated with a deep (shallow) thermocline, and in the west, warm (cold) SST is associated with a shallow (deep) thermocline. The eastern positive pattern, which can be related to an El Niño–Southern Oscillation (ENSO)-type air–sea interaction (Carton *et al.*, 1996), is interrupted by a narrow negative zonal band located along 1–3°N (between the subsurface Equatorial Counter Current and North Equatorial Counter Current at the surface), a region with complex dynamics linked to horizontal shearing (Bryan *et al.*, 1995). This behaviour appears in Figure 6, which shows the correlation at zero lag between the observed and simulated SST and Z20 anomalies along the ship track AX 15. Areas where Z20 surfaces or is very close to the coast are omitted. In a manner consistent with Figure 5, the correlation between the observed SST and Z20 anomalies is positive along

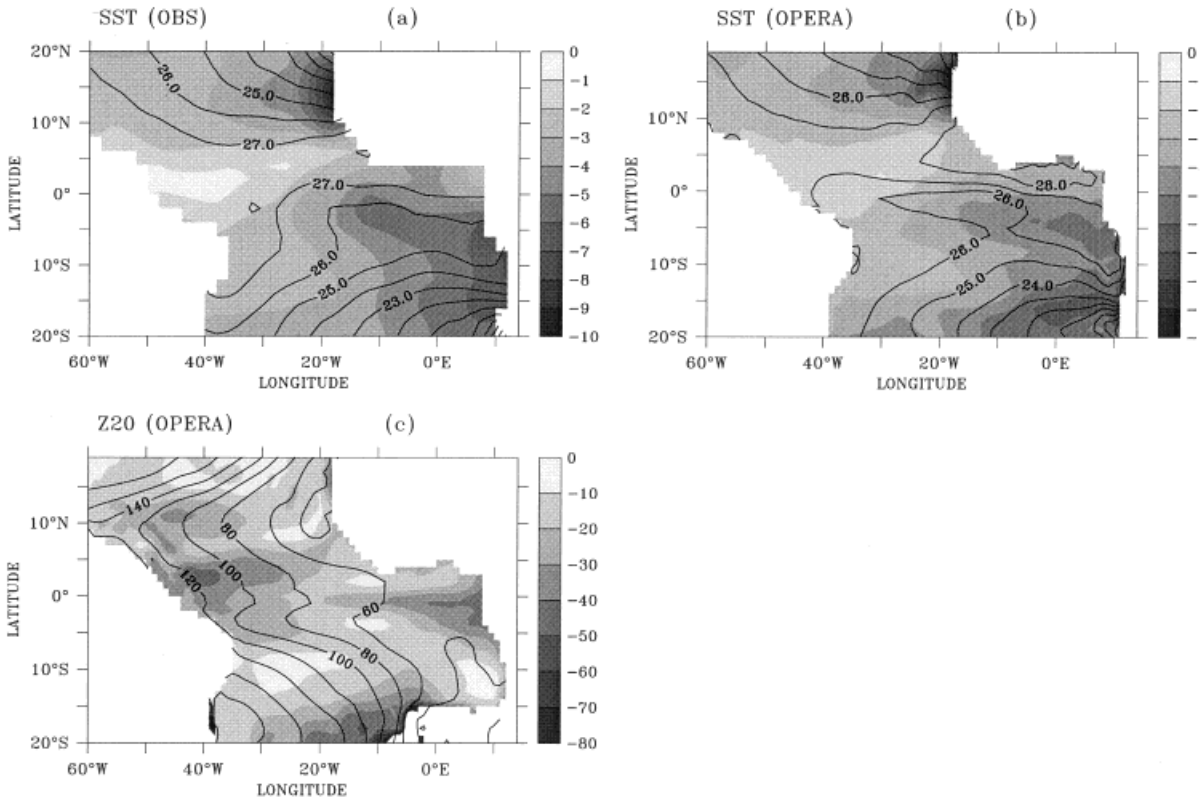

Figure 4. (a) Total average (solid lines) and seasonal range (shaded areas) of SST from the 1979–1993 monthly observations. (b) Same as (a) but for simulated SST. (c) Same as (b) but for simulated Z20. SST units are in °C, Z20 units are in m

the AX 15 ship track (10°N–9°S), with lower values in the narrow band 1–3°N, where the correlation done with simulated values is negative.

3.3. Relationship between simulated SST dipole and Z20 equatorial slope

The two main modes of climatic variability can be roughly characterized by the first vectors of two EOF analyses done on simulated SST and subsurface temperature anomaly fields, respectively. The type of anomaly used here is that one where the seasonal average is just removed, in such a way the regional variances are saved for each variables. The spatial structures of each one of the first EOFs (EOF-1) of simulated monthly anomalies of Z20 and SST can be seen in Figures 1 and 2, respectively. The range of the variance explained by the EOF-1s are similar for both variables (22% for Z20 and 23% for SST). The EOF-1 pattern associated with Z20 anomalies (Figure 1) is predominantly zonal and symmetric about the equator, consistent with the inter-annual variability pattern shown on Figure 4(c). Opposite values of Z20 variability balances from eastern to western areas, with a pivot zone close to 25°W. The simulated dipole structure associated with the inter-hemispheric gradient in SST, which can be seen in opposite signs north and south of the mean position of the ITCZ is shown in Figure 2. Superimposing the two monthly time series associated with each EOF-1 (Figure 7) it can be noticed that they have similar temporal behaviour at various inter-annual time-scales. The two series are strongly correlated, giving an MCC of $+0.66$ at 1-month lag (Z20 leading) on the monthly time series (MCC $= +0.74$ at zero lag on the 6-month smoothed time series).

In Figure 8, model results, without any statistical filtering, are shown in a similar way as the curves of observed ΔZ20 and ΔSST (see on Figure 3). The simulated ΔSST is calculated according to the same method as that used to compute the observed SST dipole (difference between TN and TS; see Figure 2).

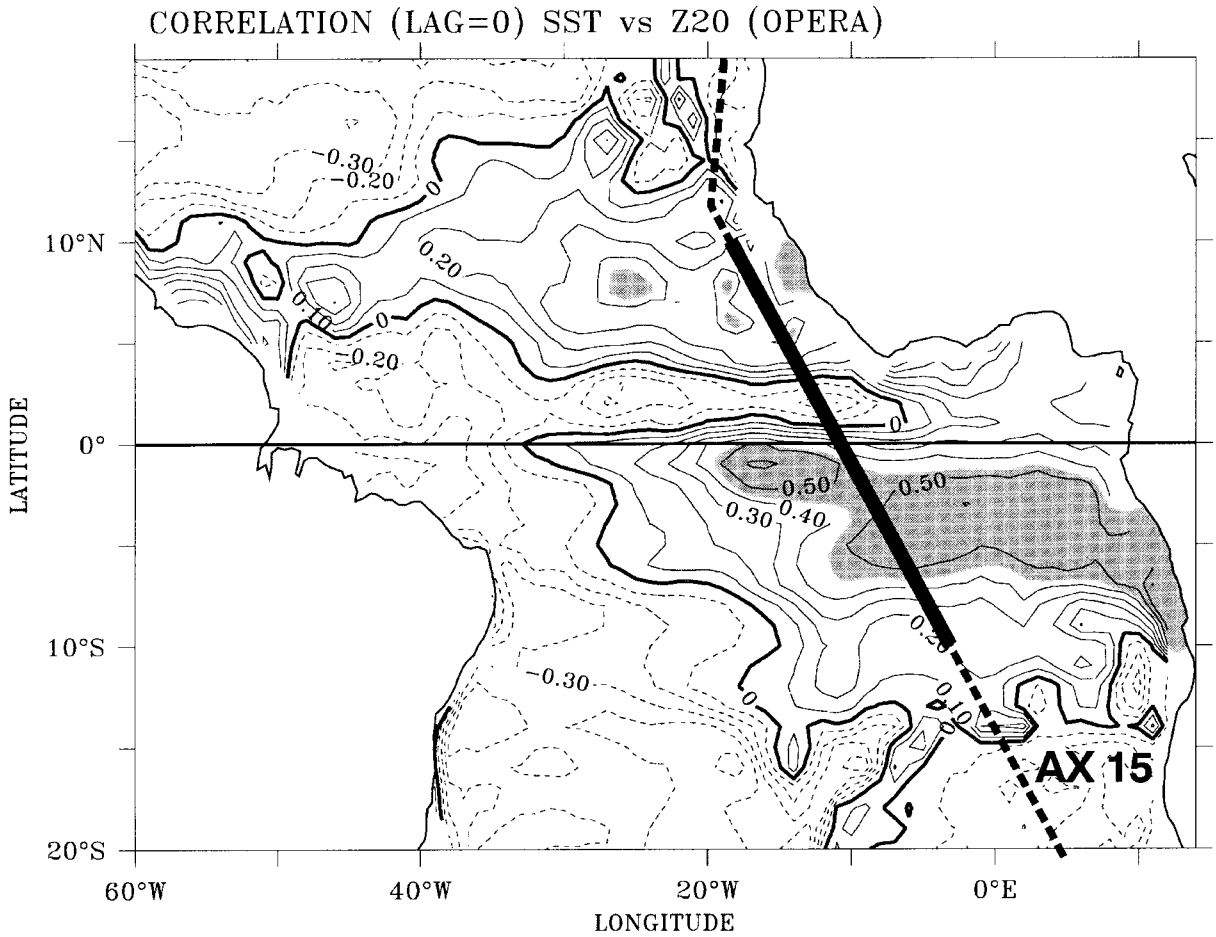

Figure 5. Correlation map at zero lag between SST and Z20 anomalies from the numerical solution. The ship track AX 15 is indicated by a thick straight line between 10°N and 10°S (where the correlation is made between Z20 and SST observed anomalies on Figure 6), and by thick dashed lines poleward of 10°N and 10°S. Positive (negative) values are represented by solid (dashed) lines. Contour interval is 0.1. Shaded areas indicate the 5% significance level

The simulated ΔZ20 is calculated using the difference between the two equatorial areas (western area, ZW, minus eastern area, ZE) delimited on Figure 1 (10°N–10°S/60°W–20°W for ZW; 5°N–5°S/20°W–20°E for ZE), which roughly correspond to the domains where the spatial EOF-1 values are the highest

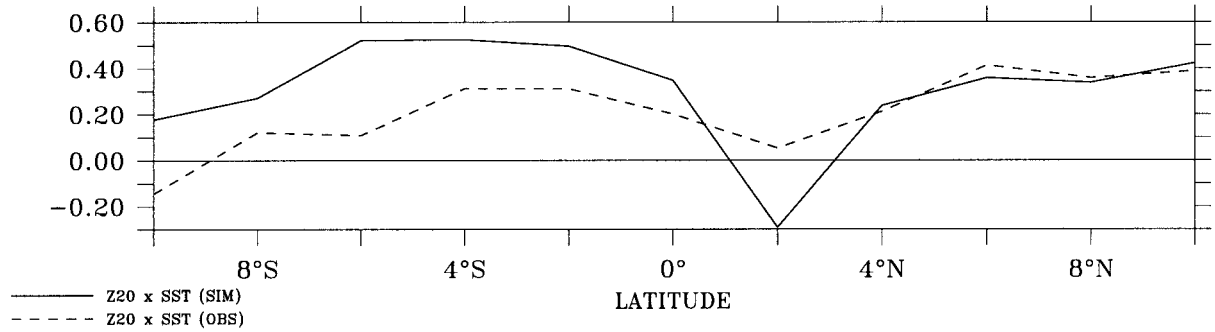

Figure 6. Correlation at zero lag between the SST and Z20 simulated (solid line) and observed (dashed line) anomalies along the ship-track AX 15 from 10°N to 10°S (see also Figure 5)

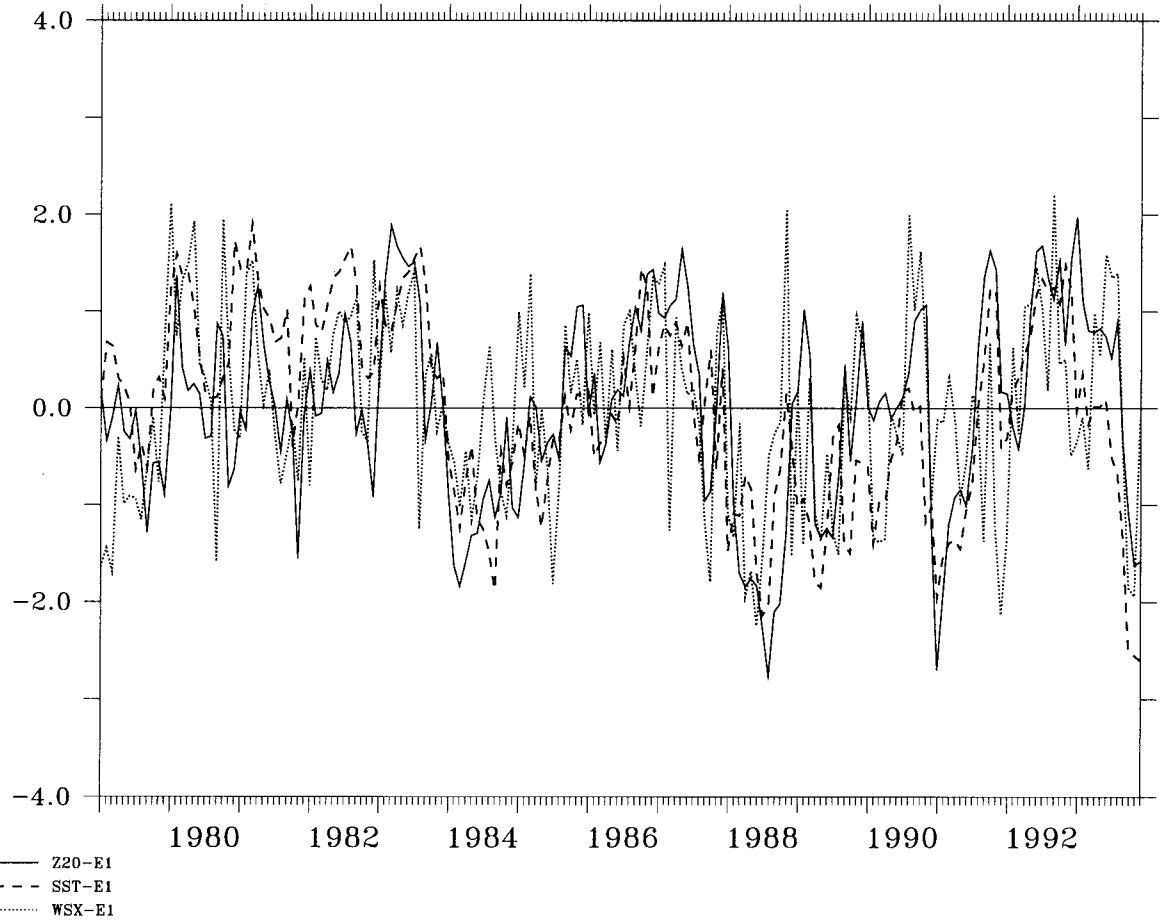

Figure 7. 1979–1993 monthly times series associated with EOF-1s of simulated Z20 anomalies (solid line), SST anomalies (dashed line), and ECMWF zonal wind stress (τ^x) anomalies (dotted line) inside the equatorial band 5°N–5°S. The EOF-1 patterns are presented on Figures 1, 2 and 9, respectively. Standard units

(see Figure 1). The MCC between ΔZ20 and ΔSST is $+0.54$ at high frequency (i.e. the 5-day output step of the model) at zero lag, to $+0.55$ for monthly values. This last value is significantly higher than the MCC provided by the same relationship computed from the observations ($+0.45$, see Figure 3). A possible explanation of that difference is that the ΔZ20 time series computed from the observations, from only two equatorial points, is only an estimation of the true value of the Z20 equatorial slope. The MCC deduced from the simulation goes up to a maximum of $+0.66$ with a 2-month lag (Z20 leading) when using a 6-month running mean. Thus, this supports the idea that the inter-annual signal provided by the numerical solution is reasonably consistent with the observations, and can be used to illustrate the main modes of inter-annual variability of the tropical Atlantic.

3.4. The role of the wind forcing in the relationship between the two climatic modes

Figure 9 shows the pattern of EOF-1 (39% of the total variance) obtained from the ECMWF reanalysis zonal wind stress (τ^x) monthly anomaly for the equatorial band between 5°N and 5°S, from coast to coast. This is the region where the dynamic forcing is of prime importance for the oceanic equatorial response (Cane and Sarachik, 1977). The monthly anomalies used here are the deviations from the seasonal mean. The highest signal occurs in the western area, where the variability is also the strongest (Servain and Arnault, 1995). The associated time series is shown in Figure 7, superimposed by the two

other curves previously discussed, and related to the monthly values of SST EOF-1 and Z20 EOF-1 time series. The MCC between the zonal equatorial τ^x, SST and Z20 monthly anomalies are: $+0.45$ at zero lag between τ^x and SST and $+0.50$ between τ^x and Z20 at 1-month lag (τ^x leading). These MCC go up to $+0.63$ and $+0.64$ with the same lags, respectively, when using the 6-month running mean filter. This indicates that equatorial dynamic forcing is linked not only to the Z20 equatorial zonal seesaw, as suggested by early works, but *also* to the SST dipole.

ΔITCZ is defined here (as in Servain *et al.*, 1999) as being the anomalous latitudinal displacement of the zero value of the meridional wind along 29°W, a meridian near the centre of the basin. Positive/negative values of ΔITCZ identify its northward/southward anomalous position of ITCZ. Figure 10, computed here from the numerical solution, is similar to Figure 3 of Servain *et al.* (1999), which was computed from merchant ship observations. Using the 6-month smoothed values, the MCC between simulated ΔITCZ (from ECMWF reanalysis) and the simulated ΔZ20 is $+0.55$ at a 2-month lag (ΔZ20 leading). It was $+0.45$ at zero lag from the observations (Servain *et al.*, 1999). The MCC between simulated ΔITCZ and simulated ΔSST is $+0.47$ at zero lag. It was $+0.73$ with 1-month lag (ΔITCZ leading) from the observations (Servain *et al.*, 1999). The reason of the differences between the results from the simulation and from the observations, especially in the lags for MCC computed from smoothed time-series, is not clear and needs further investigations. The MCCs are weaker when using the non-smoothed monthly values ($+0.27$ and $+0.30$, respectively) because of the spurious high frequency

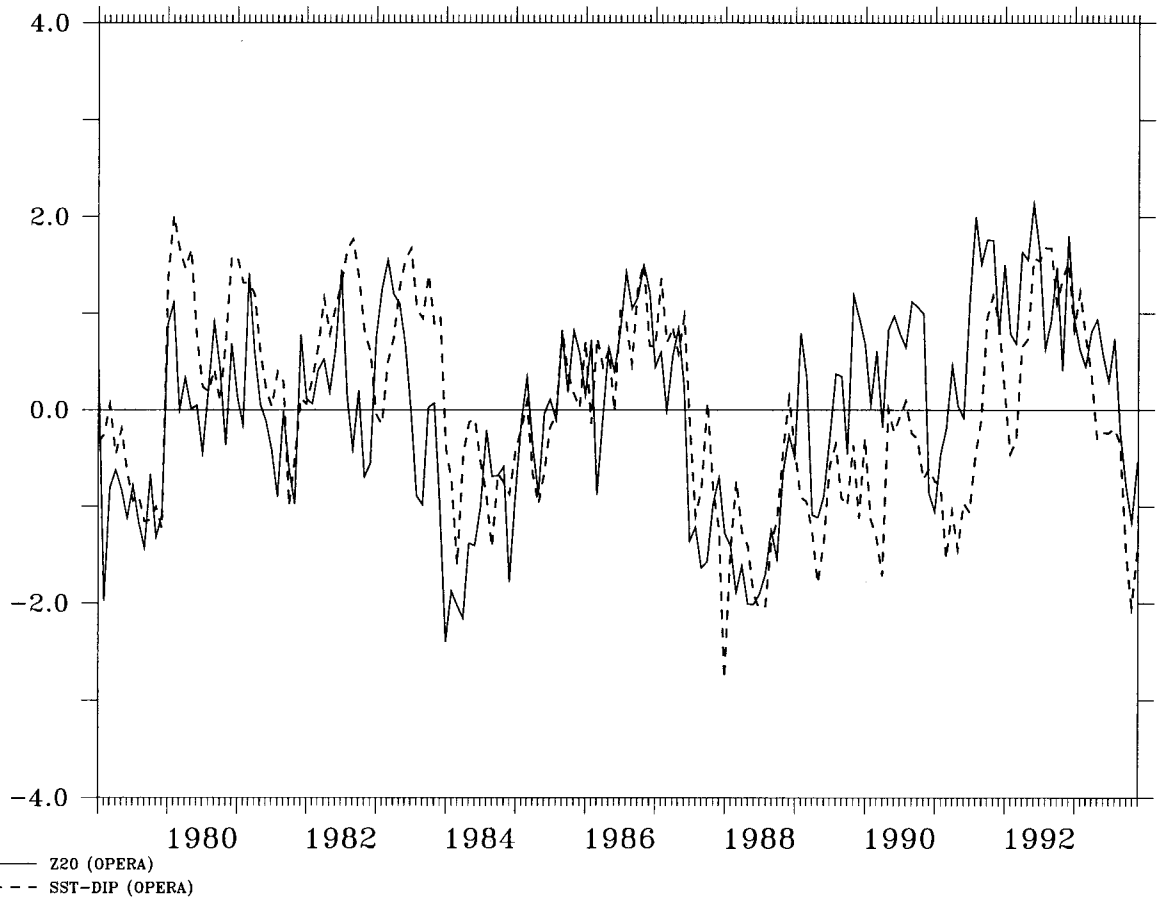

Figure 8. 1979–1993 time series of ΔZ20 (solid line) and ΔSST (dashed line) indices, calculated from the numerical solution. ΔZ20 and ΔSST are related to the differences between areas shown in Figure 1 (ZW minus ZE) and Figure 2 (TN minus TS), respectively. Standard units

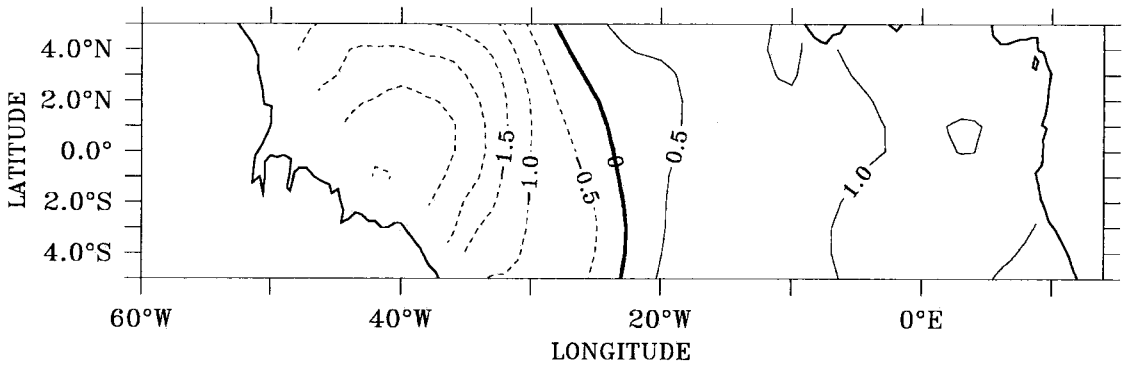

Figure 9. Spatial structure of EOF-1 of the zonal wind stress (τ^x) monthly anomalies from the ECMWF reanalysis in the equatorial Atlantic area limited by the latitude 5°N and 5°S. Contour interval (positive in solid lines, negative in dashed lines) is 0.5 in standard units

occurring in the wind stress outputs of the ECMWF reanalysis. Nevertheless, the time lags for these MCC, both at zero lag, are in better agreement with the observations (Servain *et al.*, 1998b, 1999).

4. CONCLUSION

The above study reinforces the idea that the dynamics, especially the slow ones, are of prime importance in understanding the processes governing the inter-annual variability of the entire tropical Atlantic climate. Indeed, the two main modes of inter-annual variability traditionally observed in the tropical Atlantic—not only the equatorial dynamical mode, as has been known for many years, but *also* the meridional SST mode—are directly forced by large-scale atmospheric fluctuations occurring within both hemispheres, via the full trade wind system. Until now it was assumed that the inter-annual variations in the equatorial slope of the thermocline were directly forced by the wind (via linear dynamic processes), while the inter-annual variations in the SST dipole were supposed as the main response of complex thermodynamic processes including turbulent and radiative exchanges, and other advective processes in the entire subtropical domain. In this work, it is suggested that it is the anomalous fluctuations in the entire trade wind system that are inducing inter-hemispheric SST anomaly patterns (as a response). In other words, the results (see Figure 7) show that the north–south SST fluctuations in the tropical Atlantic can be simply addressed by the wind forcing inside the equatorial band, which is the prevailing cause for the equatorial oceanic response.

In fact, it seems that the inter-annual variability of climate in the tropical Atlantic follows the same rules as that of the annual cycle. A possible scenario would be the following. Imagine an anomalous southward displacement of the ITCZ in phase with enhanced northeast trades and weaker southeast trades. The southward position of the ITCZ induces weaker equatorial winds (especially the zonal wind in the west). This would affect the thermocline depth along the equator with an abnormal elevation at the western side of the basin and an abnormal deepening in the east, then inducing a flatness in the zonal slope. This pattern induces (Servain and Arnault, 1995; Nobre and Shukla, 1996) cold SST anomalies towards the northern side of the basin (more evaporation), and warm SST anomalies in all the equatorial (especially inside the Gulf of Guinea) and southern oceanic domains (less evaporation). This situation associates an El Niño-type Atlantic event (warming of Gulf of Guinea) with a negative SST Atlantic dipole index (cold to the North, warm to the South). Such a climatic episode is one condition to favour enhanced rainfall in the Nordeste region and along the continental border of the Gulf of Guinea, and drought in the Sahel.

The correlation coefficients found in this numerical study are generally higher than those previously reported in an observational study of the same topic (Servain *et al.*, 1998b, 1999). This can be explained

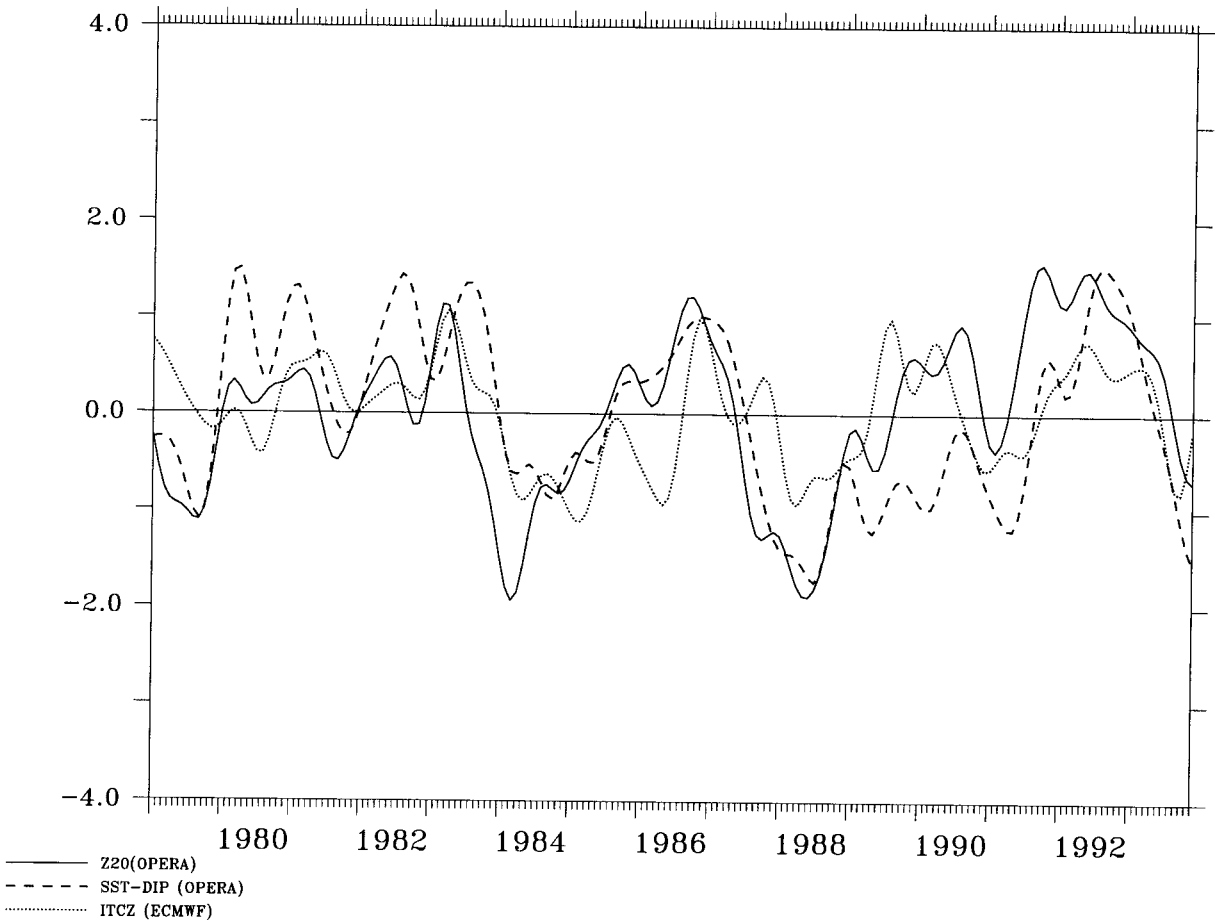

Figure 10. 1979–1993 6-month smoothed time series of ΔZ20 (solid line), ΔSST (dashed line), and ΔITCZ (dotted line) indices, calculated from the numerical solution. ΔZ20 and ΔSST are related to the areas shown in Figure 1 (ZW minus ZE) and Figure 2 (TN minus TS), respectively. ΔITCZ is estimated along 29°W (see the text for details of calculation). Standard units

in terms of the availability of observations, especially those related to the thermocline depth. Undeniably, the continuous flow of outputs from numerical models allows us to build time-series according to a technique distinctively more homogeneous than those using the *in situ* data. This induces reduction of the associated noise and, consequently, enhances the correlation between them.

Though the present results are consistent with those obtained from observations, some points remain unclear, especially in the time-lags of the various responses. Further work is necessary to improve the understanding of the balance between the dynamic and the thermodynamic systems responsible for the generation of the equatorial and meridional climatic modes of the tropical Atlantic. Another study is already underway with the objective of estimating the relationships between the Atlantic indices studied here and other climatic indices, with emphasis on the Southern Oscillation index.

ACKNOWLEDGEMENTS

The authors express thanks to Alain Dessier who provided the XBT time series, and are grateful to the two reviewers for their comments. This work was supported by COFECUB agreement No. 27/96-99 and by CNPq grant 300223/93-5 RN. Graphics were done by using Ferret.

REFERENCES

Binet D. 1982. Influence des variations climatiques sur la pêcherie des Sardinella aurita ivoiro- ghanéenne: relation sécheresse-surpêche. *Oceanologica Acta* **5**: 443–452.

Binet D, Marchal E. 1993. The large marine ecosystem of shelf areas in the Gulf of Guinea: long-term variability induced by climatic changes. In *Large Marine Ecosystems*: *Stress*, *Mitigation and Sustainability*. Publication 92-395, Sherman K, Alexander LW, Gold BD (eds). Association for the Advancement of Science Press; 104–118.

Bryan FO, Wainer I, Holland WR. 1995. Sensitivity of the tropical Atlantic circulation to specification of wind stress climatology. *Journal of Geophysical Research* **100**(24): 729–744.

Cane MA, Sarachik ES. 1977. Forced baroclinic ocean motions. II. The linear equatorial bounded case. *Journal of Marine Research* **35**: 395–432.

Carton JA, Cao X, Giese BS, da Silva AM. 1996. Decadal and interannual SST variability in the tropical Atlantic. *Journal of Physical Oceanography* **26**: 1165–1175.

Carton JA, Huang B. 1994. Warm events in the tropical Atlantic. *Journal of Physical Oceanography* **24**: 888–893.

Chang P, Ji L, Li H. 1997. A decadal climate variation in the tropical Atlantic Ocean from thermodynamic air–sea interactions. *Nature* **385**: 516–518.

Delécluse P, Madec G, Imbard M, Levy C. 1993. OPA version 7 ocean general circulation model reference manual. *Rapport Interne LODYC 93/05*; 1–111 (Available from LODYC, Université Paris VI, 75252 Paris, France).

Delworth TL, Mehta VM. 1998. Simulated interannual to decadal variability in the tropical and sub-tropical Atlantic. *Geophysical Research Letters* **25**: 2825–2828.

Enfield DB, Mestas-Nuñez AM, Mayer DA, Cid-Serrano L. 1999. How ubiquitous is the dipole relationship in tropical Atlantic sea surface temperatures? *Journal of Geophysical Research* **104**: 7841–7848.

Fabri MC, Dessier A, Maudire G, Raguenes Y, Rebert J-P. 1996. Global subsurface data centre (GSDC) for TOGA and WOCE. *International WOCE Newsletter* **22**: 18–20.

Fontaine B, Bigot S. 1993. West African rainfall deficits and sea surface temperatures. *International Journal of Climatology* **11**: 271–286.

Fontaine B, Janicot S, Moron V. 1995. Rainfall anomaly patterns and wind field signals over West Africa in August (1958–1989). *Journal of Climate* **8**: 1503–1508.

Fonteneau A. 1991. Les anomalies de l'environnement en 1984 dans le Golfe de Guinée. Effets possibles sur la capturabilté de l'albacore. *Rec. Doc. Scient. International Commission for the Conservation of Atlantic Tuna*, *Standing Committee for Research and Statistics* **XXXVI**: 380–408.

Harzallah A, Rocha de Aragão J, Sadourny R. 1996. Interannual rainfall variability in northeast Brazil: observation and model simulation. *International Journal of Climatology* **16**: 861–878.

Hastenrath S. 1978. On modes of tropical circulation and climate anomalies. *Journal of Atmospheric Science* **35**: 2222–2231.

Hisard P. 1980. Observation de réponses de type 'El Nino' dans l'Atlantique tropical, Golfe de Guinée. *Oceanologica Acta* **3**: 69–78.

Houghton RW. 1991. The relationship of sea surface temperature to thermocline depth at annual and interannual time scales in the tropical Atlantic Ocean. *Journal of Geophysical Research* **96**: 15 173–15 185.

Houghton RW, Tourre YM. 1992. Characteristics of low-frequency sea surface temperature fluctuations in the tropical Atlantic. *Journal of Climate* **5**: 765–771.

Kallberg P. 1995. ECMWF reanalysis project. WCRP Workshop on Air–Sea Flux Fields for Forcing Ocean Models and Validating GCMS, ECMWF, UK, 24–27 October.

Katz EJ. 1987. Equatorial Kelvin waves in the Atlantic. *Journal of Geophysical Research* **92**: 1894–1898.

Katz EJ. 1997. Waves along the equator in the Atlantic. *Journal of Physical Oceanography* **27**: 2536–2544.

Lamb PJ. 1978a. Large-scale tropical Atlantic surface circulation anomalies associated with sub-Saharan weather anomalies. *Tellus* **30**: 240–251.

Lamb PJ. 1978b. Case studies of tropical Atlantic surface circulation pattern during recent sub-Saharan weather anomalies: 1967 and 1968. *Monthly Weather Review* **106**: 482–491.

Levitus S. 1982. Climatological atlas of the World Ocean. *NOAA Prof. Paper 13*, US Government Printing Office, Washington DC.

McCreary JP, Picaut J, Moore DW. 1984. Effects of remote annual forcing in the eastern tropical Atlantic Ocean. *Journal of Marine Research* **42**: 45–81.

McPhaden MJ. 1993. TOGA-TAO and the 1991–1993 El Niño–Southern Oscillation event. *Oceanography* **6**: 36–44.

Mehta VM, Delworth T. 1995. Decadal variability of the tropical Atlantic Ocean surface temperature in shipboard measurements and in a global ocean–atmosphere model. *Journal of Climate* **8**: 172–190.

Merle J. 1980. Variabilité thermique annuelle et interannuelle de l'océan atlantique équatorial est, l'hypothèse d'un 'El Niño' Atlantique. *Oceanologica Acta* **3**: 209–220.

Merle J, Fieux M, Hisard P. 1980. Annual signal an interannual anomalies of sea surface temperature in the eastern equatorial Atlantic. *Deep Sea Research* **26**(GATE suppl. II): 77–101.

Merle J, Arnault S. 1985. Seasonal variability of the surface dynamic tpography in the tropical Atlantic Ocean. *Journal of Marine Research* **43**: 267–288.

Moore DW, Hisard P, McCreary J, Merle J, O'Brien J, Picaut J, Verstraete JM, Wunsch C. 1978. Equatorial adjustment in the eastern Atlantic. *Geophysical Research Letters* **5**: 637–640.

Moron V, Bigot S, Roucou P. 1995. Rainfall variability in subequatorial America and Africa and relationships with the main SST modes (1951–1990). *International Journal of Climatology* **15**: 1297–1322.

Moron V, Vautard R, Ghil M. 1998. Trends, interdecadal and interannual oscillations in global sea–surface temperatures. *Climate Dynamics* **14**: 545–569.

Moura AD, Shukla J. 1981. On the dynamics of droughts in northeast Brazil: observations, theory and numerical experiments with a general circulation model. *Journal of Atmospheric Science* **38**: 2653–2675.

Nobre P, Shukla J. 1996. Variations of sea surface temperature, wind stress, and rainfall over the tropical Atlantic and South America. *Journal of Climate* **9**: 2464–2579.
Philander SGH. 1979. Variability of the tropical oceans. *Dynamics of Atmosphere and Ocean* **3**: 191–208.
Philander SGH, Pacanowsky RC. 1981. The ocean response to cross-equatorial winds. *Tellus* **33**: 201–210.
Picaut J. 1983. Propagation of the seasonal upwelling in the eastern equatorial Atlantic. *Journal of Physical Oceanography* **13**: 18–37.
Rao VB, Chapa SR, Franchito SH. 1999. Decadal variation of atmosphere–ocean in the tropical Atlantic and its relationship to the northeast Brazil rainfall. *Journal of the Meteorological Society of Japan* **77**: 63–75.
Reverdin G, Delécluse P, Lévy C, Andrich P, Morlière A, Verstraete JM. 1991. The near surface tropical Atlantic in 1982–1984. Results from a numerical simulation and a data analysis. *Progress in Oceanography* **27**: 273–340.
Reynolds RW, Smith TM. 1994. Improved global sea surface temperature analyses using optimum interpolation. *Journal of Climate* **7**: 929–948.
Servain J. 1991. Simple climatic indices for the tropical Atlantic Ocean and some applications. *Journal of Geophysical Research* **96**: 15 137–15 146.
Servain J, Arnault S. 1995. On forecasting abnormal climatic events in the tropical Atlantic Ocean. *Annales Geophysicae* **13**: 995–1008.
Servain J, Lukas S. 1990. *Climatic Atlas of the Tropical Atlantic Wind Stress and Sea Surface Temperature 1985–1989*. Service de la Documentation et des Publications (S.D.P.), IFREMER, Plouzané, France; 1–133.
Servain J, Picaut J, Busalacchi AJ. 1985. Interannual and seasonal variability of the tropical Atlantic Ocean depicted by sixteen years of sea surface temperature and wind stress. In *Coupled Ocean–Atmosphere Models*, Nihoul JCJ (ed). Elsevier Science: Amsterdam; 211–237.
Servain J, Busalacchi AJ, McPhaden MJ, Moura AD, Reverdin G, Vianna M, Zebiak SE. 1998a. A pilot research moored array in the tropical Atlantic (PIRATA). *Bulletin of the American Meteorological Society* **79**: 2019–2031.
Servain J, Wainer I, Dessier A. 1998b. Evidence d'une liaison entre les deux principaux modes de variabilité climatique interannuelle de l'Atlantique tropical. CR Acadamy of Sciences, Paris. *Sciences de la Terre et des Planètes* **327**: 1–8.
Servain J, Wainer I, McCreary JP, Dessier A. 1999. Relationship between the equatorial and meridional modes of climatic variability in the tropical Atlantic. *Geophysical Research Letters* **26**: 485–488.
Smith TM, Chelliah M. 1994. Atlas of the tropical Pacific Ocean annual cycle. *NOAA Atlas*, **13**, US Department of Commerce, NOAA/NWS, Camp Springs, MD; 1–64.
Tanimoto Y, Xie SP. 1999. Ocean–atmosphere variability over the Pan-Atlantic basin. *Journal of the Meteorological Society of Japan* **77**: 31–46.
Wagner RG. 1996. Decadal-scale trends in mechanisms controlling meridional sea surface temperature gradients in the tropical Atlantic. *Journal of Geophysical Research* **101**: 16 683–16 694.
Wagner RG, da Silva A. 1994. Surface conditions associated with anomalous rainfall in the Guinea coastal region. *International Journal of Climatology* **14**: 178–199.
Wainer I, Soares J. 1997. North Northeast Brazil rainfall and its decadal—scale relationship to wind stress and sea surface temperature. *Geophysical Research Letters* **24**: 277–280.
Zebiak SE. 1993. Air–sea interaction in the equatorial Atlantic region. *Journal of Climate* **6**: 1567–1586.

